IEEE Access
Multidisciplinary ⋮ Rapid Review ⋮ Open Access Journal

Received 19 March 2023, accepted 4 April 2023, date of publication 7 April 2023, date of current version 12 April 2023.

Digital Object Identifier 10.1109/ACCESS.2023.3265478

RESEARCH ARTICLE

Nonlinear Transient Mathematical Model of Large-Capacity Synchronous Condenser Based on Time-Varying Reactance Parameters

XIAO HAN, YANPING LIANG, ERHANG ZHU, AND XU BIAN
College of Electrical and Electronic Engineering, Harbin University of Science and Technology, Harbin 150080, China
Corresponding author: Yanping Liang (liangyanping2010@126.com)

This work was supported in part by the Natural Science Foundation of Heilongjiang Province of China under Grant ZD2019E008.

ABSTRACT Large-capacity synchronous condenser (SC) is an essential dynamic reactive power compensation device in an Ultra-high voltage direct current (UHVDC) transmission system. The particular transient operating state and structural characteristic of SC lead to a severe magnetic saturation effect during transient operation. To accurately describe the dynamic characteristics of SC, it is urgent to establish a transient mathematical model considering the magnetic saturation effect. Therefore, this paper proposes a nonlinear transient mathematical model for SC based on time-varying reactance parameters and gives a calculation method for time-varying reactance parameters. The mathematical model proposed in this paper is verified by taking a 300MVar SC as the research object. This condenser is connected to the power grid at the sending end of the UHVDC transmission system. The proposed mathematical model, the traditional fixed-parameter transient mathematical model, and the saturated standard SG model used in the power system were used to simulate the voltage generated by dynamic reactive power compensation characteristics of SC during a drop failure. Compared with the fault test results, the accuracy of the proposed mathematical model is verified. The effect of magnetic saturation on the dynamic reactive power compensation characteristics was analyzed, respectively. In addition, the accuracy of the proposed mathematical model is closer to the actual motor state, which is helpful for further research on the operation analysis and state monitoring of SC.

INDEX TERMS Synchronous condenser, nonlinear transient mathematical model, time-varying parameter, magnetic saturation effect, reactive power compensation.

I. INTRODUCTION

The UHVDC transmission system suffers from fault problems such as voltage instability and insufficient dynamic reactive power reserves [1], [2]. SC has strong reactive power support and overload capacity during transient operation and can provide dynamic reactive power compensation to maintain grid voltage stability in case of serious voltage sag [3], [4]. However, unlike traditional synchronous condensers, large-capacity synchronous condensers operate in transient mode as the primary mode of operation. When the power grid fails, the impact current will cause a severe magnetic saturation effect on the iron core of the synchronous condenser, which will lead to motor failure. An accurate and efficient mathematical model is the basis for fault condition monitoring and operational analysis of the SC. Therefore, to accurately calculate the dynamic behavior of the SC during a system failure, a high precision, the SC transient mathematics needs to be established.

There are two types of modeling methods for transient mathematical models, one type is the finite element method (FEM), and the other type is the analytical method. FEM is based on the physical model of the motor to construct a finite element model to simulate the operating conditions of the motor, which can take into account the nonlinear factors of the dynamic process and has high calculation accuracy [5]. However, FEM is computationally expensive, and the simulation time required for one run is too long for a large-capacity

The associate editor coordinating the review of this manuscript and approving it for publication was Emanuele Crisostomi.

synchronous condenser connected in parallel to a complex grid system. The analytical method is to equate the motor as two sets of coils with relative motion and mutual coupling, to establish the mathematical equations based on the laws of the circuit and magnetic circuit, to calculate the parameters in the mathematical equations in combination with FEM, and to obtain a transient mathematical model to characterize the dynamic behavior of the motor. The analytical method is widely used because of its low computational cost and high efficiency [6]. The synchronous generator model based on Park equation transformation is a classical analytical model for the dynamic analysis of synchronous motors. On this basis, many analytical models considering the saturation characteristics of motors have been proposed. The literature [7] uses an analytical method of finite-element-state-space coupling, combining FEM with the equation of the state of the motor, to establish a transient mathematical model of the motor, taking into account the saturation characteristics of the parameters. Literature [8], [9], [10] shows that most of the dynamic models of conventional power generation units are based on the analytical models of models 2.1 and 2.2 described in IEEE Standard 1110-2019. In the process of large disturbance simulation, the saturation characteristics of the motor are considered by adjusting the excitation inductance Lad and Laq. However, studies on analytical modeling have mainly focused on considering the saturation characteristics of armature reaction reactance [11], [12], with fewer studies considering the saturation characteristics of transient reactance. The transient reactance parameter is of a leakage reactance nature, and the reactance parameter in the analytical method of modeling consists of a leakage reactance and an armature reaction reactance. Transient reactance is the critical technical parameter affecting the dynamic reactive power compensation characteristics of SC [13], [14]. Therefore, an accurate calculation considering the transient reactance is a prerequisite for an accurate analysis of the SC during transient operation. Currently, the transient reactance parameters are solved using specific identification methods, including time domain identification [15], [16] and frequency domain identification [17], [18], [19], [20], [21]. The transient parameters obtained by these calculation methods are fixed constants even when magnetic saturation characteristics are taken into account and are suitable for motors with mainly steady-state operations. It cannot meet the needs of dynamic operation analysis of the SC during UHVDC system faults. To more accurately reflect the transient process of voltage sag during system faults and to accurately describe the dynamic reactive power compensation characteristics, a non-linear transient mathematical model for the SC that considers the change in reactance with saturation characteristics needs to be established.

In this paper, a new nonlinear transient mathematical model of a large-capacity synchronous condenser is established, and the calculation method of the time-varying reactance parameters in the mathematical model is proposed.

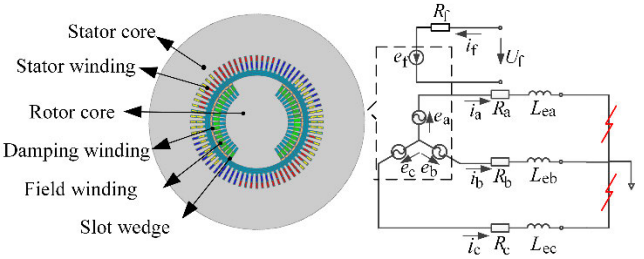

FIGURE 1. Finite element model of no-load three-phase sudden short circuit of SC.

In order to verify the proposed mathematical model, the simulation results of the nonlinear, the saturated standard SG model used in the power system and the traditional fixed-parameter mathematical model are compared and analyzed with the field test results, taking the voltage sag fault of the UHVDC transmission system as an example.

II. CALCULATION METHOD OF TIME-VARYING REACTANCE PARAMETERS

Reactance parameters are essential parameters for building a transient mathematical model. This paper analyzes the effect of dynamic magnetic saturation on reactance parameters during the transient operation of SC. And the saturation characteristic curve family of reactance parameters is constructed. Then the neural network models for different reactances are obtained using BP neural networks based on curve families. The neural network models for different reactances will later be used to characterize the time-varying reactance parameters in the transient mathematical model.

A. EFFECT OF DYNAMIC MAGNETIC SATURATION ON REACTANCE

The transient mathematical model is established to accurately analyze the dynamic characteristics of SC when it is subjected to large disturbances. In this paper, a typical large disturbance condition of a no-load three-phase sudden short circuit is used as an example to analyze the dynamic magnetic saturation.

The simulation model is shown in Fig. 1. e_a, e_b, e_c, and e_f are the electromotive force of the stator and field winding, respectively. R_a, R_b, R_c, and R_f are resistances. i_a, i_b, i_c, and i_f are currents. L_{ea}, L_{eb}, and L_{ec} are the end inductances of the stator winding. U_f is the voltage of the field winding. Eddy current effects in the rotor core, slot wedge, and damping winding are considered.

μ_r is the relative magnetic permeability. Based on the simulation model in Fig. 1 established by the finite element software transient field, this paper obtains the relative permeability distribution of the stator and rotor core at different short circuit times of SC, as shown in Fig. 2. The smaller the relative permeability, the higher the degree of magnetic saturation of the core. From the relative permeability distribution at 0.01s, 0.09s, and 0.99s after the short circuit,

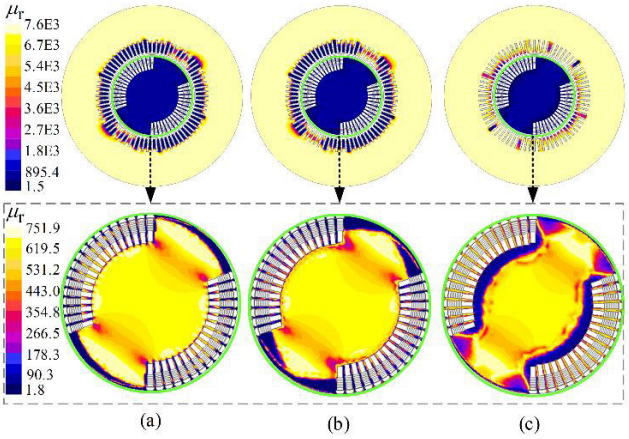

FIGURE 2. Relative permeability distribution of stator and rotor cores at different moments of short circuit. (a) 0.01s. (b) 0.09s. (c) 0.99s.

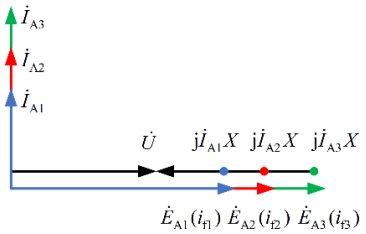

FIGURE 3. Phasor diagram of SC operating state.

it can be seen that the locations of severe magnetic saturation are concentrated in the teeth of the stator core and the large teeth of the rotor core. The magnetic saturation of the stator core teeth decreases with increasing short-circuit time. The rotor core teeth gradually spread to the inside of the core and decrease with increasing short-circuit time. As a result, SC has a dynamic magnetic saturation effect during transient operation, and the relative permeability distribution of the core is complex and changes with the transient operation.

The reactance parameter is a concentration parameter reflecting the magnetic field, which can be obtained from equation (1):

$$X = \omega L = \frac{\omega N^2 A}{l}\mu \tag{1}$$

where ω is the angular frequency, L is the inductance, N is the number of turns of the winding, A is the cross-sectional area, and l is the length of the magnetic circuit. In general, with ω, N, A, and l being constants, the relationship between X and μ is shown in equation (2):

$$X = f(\mu) \tag{2}$$

In equation (2), the reactance parameter changes with the core permeability. However, the distribution of core permeability is complex, and equation (2) is not easily expressed directly. According to the properties of the core ferromagnetic material and the Ampere loop theorem, the magnetic permeability μ of the core maps to the magnetic field strength H,

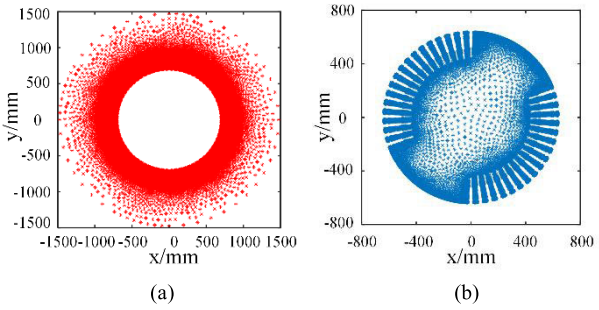

FIGURE 4. Freezing position of relative magnetic permeability. (a) Stator core. (b) Rotor core.

which in turn maps to the winding current i. Thus, the mapping relationship between reactance and permeability can be characterized by a mapping relationship between reactance and current.

The phase diagram of the operating state during SC over- excitation is shown in Fig. 3. Where $\dot{U}$ represents the voltage phase at the end of the regulator, $\dot{E}_{A1}$ represents the electromotive force corresponding to the field current i_{f1}. $\dot{E}_{A2}$ represents the electromotive force related to the field current i_{f2}. $\dot{E}_{A3}$ represents the electromotive force connected to the field current i_{f3}. $\dot{I}_{A1}$, $\dot{I}_{A2}$, and $\dot{I}_{A3}$ represents the three states of the armature current of the condenser, respectively.

As seen in Fig. 3, the operating state of SC depends on the armature current and the field current. When the dynamic saturation effect is considered, the reactance parameter forms a function of the currents, as shown in equation (3):

$$X = g(i_a, i_b, i_c, i_f) \tag{3}$$

In equation (3), i_a, i_b, i_c, and i_f are time-varying during SC transient operation. Therefore, the reactance is a time-varying reactance.

B. FAMILY OF CHARACTERISTIC SATURATION CURVES FOR REACTANCE PARAMETERS

As the SC is a synchronous machine for a particular operation, the dq0 mathematical model can be used. In the modeling, one equivalent damping winding, D, is used on the d-axis of the rotor, and two equal damping windings, Q and H, are used on the q-axis, considering the eddy current effect in the rotor core. The reactance in the dq0 mathematical model contains X_d, X_f, X_D, X_q, X_Q, and X_H. Where X_d is the d-axis synchronous reactance, X_f is the field reactance, X_D is the d-axis damping winding reactance, X_q is the q-axis synchronous reactance, X_Q is the q-axis first equivalent damping reactance, and X_H is the q-axis second equivalent damping reactance. However, these reactances are not easily solved directly. In this paper, these reactances are obtained indirectly by solving for the transient reactance. Transient reactance includes X'_d, X''_d, X'_q, and X''_q. Where X'_d is the d-axis transient reactance, X''_d is the d-axis sub-transient reactance, X'_q is the q-axis transient reactance, and X''_q is the q-axis sub-transient reactance.

This section is based on the freezing permeability method to obtain numerical results of the transient reactance for different armature and field currents. The frozen position of the relative permeability of the iron cores is shown in Fig. 4.

The simulation model of Fig. 1 is used. When the rotor d-axis coincides or becomes 90° to the A phase winding axis, the relative permeability of each profiled grid of the stator and rotor cores is extracted and saved separately to obtain the d-axis and q-axis magnetic field distributions.

A constant field model is used to solve for X_{d}. The d-axis of the rotor is set to coincide with the axis of the A phase winding. The field winding is set to open-circuit. The stator winding is fed with a d-axis current to establish a d-axis magnetomotive force, at which point the d-axis current is equal to the A phase winding current. The magnetic linkage of the A phase belt is obtained through the magnetic field generated by the d-axis magnetomotive force. The formula for calculating the d-axis reactance is shown in equation (4):

$$\begin{cases} \psi_\beta = \sum_{k=1}^{q} (A_{\mathrm{U}k} - A_{\mathrm{L}k}) l_{\mathrm{ef}} \\ \psi_{\mathrm{d}} = \dfrac{\beta \times \psi_\beta}{a} \\ X = \omega \dfrac{\psi_{\mathrm{d}}}{I_{\mathrm{d}}} + X_{\sigma \mathrm{e}} \end{cases} \tag{4}$$

In equation (4), q is the number of slots per pole and per phase of the stator. $A_{\mathrm{U}k}$ and $A_{\mathrm{L}k}$ denote the magnetic vector potential at the center of the upper and lower conductors of the kth coil of the A phase winding, respectively. l_{ef} is the effective length of the stator, and ψ_{d} is the d-axis magnetic linkage. β is the number of phase belts per phase in series, a is the number of parallel branches, and ψ_β is the magnetic linkage of one phase belt. I_{d} is the incoming d-axis current, and $X_{\sigma e}$ is the stator end leakage reactance.

The eddy current field model was used to solve for the d-axis transient reactance X'_{d}. The field winding is set to short circuit, and the damping winding, rotor slot wedge, and rotor core are not considered for eddy current effects. The stator winding is fed with a d-axis current to establish the magnetomotive force of the d-axis at high frequencies and to obtain the A phase belt magnetic linkage. X'_{d} is obtained according to equation (4). In the same way, X''_{d} is obtained when the eddy current effects are considered for the damping winding, the rotor slot wedge, and the rotor core.

The rotor d-axis forms a 90° angle with the axis of the A-phase winding. X_{q}, X'_{q}, and X''_{q} are obtained using the same method for calculating the d-axis reactance.

The reactance parameters, armature currents, and field current for different states are obtained from the above method. Together, they form a family of characteristic saturation curves for different reactance parameters, as shown in Fig. 5.

C. BP NEURAL NETWORK CONSTRUCTION WITH TIME-VARYING PARAMETERS

BP neural network is a neural network that achieves feed-forward correction through error backpropagation. It can

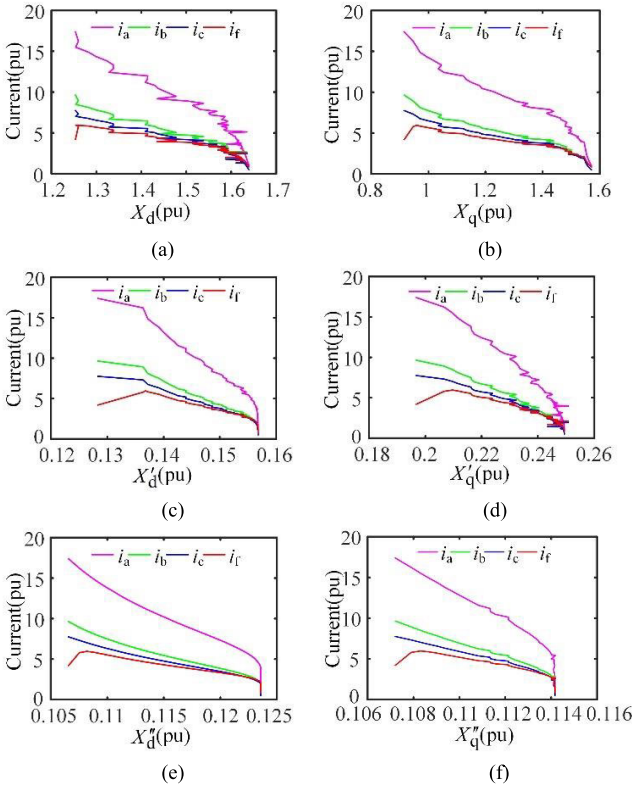

FIGURE 5. Family of characteristic saturation curves for different reactance parameters. (a) Saturation characteristic curve family of X_{d}. (b) Saturation characteristic curve family of X_{q}. (c) Saturation characteristic curve family of X'_{d}. (d) Saturation characteristic curve family of X'_{q}. (e) Saturation characteristic curve family of X''_{d}. (f) Saturation characteristic curve family of X''_{q}.

reach a non-linear mapping function from the input signal to the output signal. It can approximate arbitrary nonlinear functions, making it the preferred choice for constructing non-linear functions of multi-dimensional variables. An input layer, a hidden layer, and an output layer containing several neurons form a neural network model. The direction of signaling is from the input signal through the hidden layer to the output layer. When the output is in error with the desired result, the error is used to adjust the weights and bias to bring the creation closer to the desired result.

A family of characteristic saturation curves with different reactance parameters is used as a data set. A BP neural network is trained to obtain a neural network model with different reactances. The BP neural network model consisting of reactance parameters and multidimensional current variables is shown in Fig 6. The input layer signals are currents i_{a}, i_{b}, i_{c}, and i_{f}, and the output layer signal is time-varying reactance parameter $\hat{X}$.

In Fig. 6(a), the number of neurons in the input and output layers are j and m, respectively. The number of neurons in the hidden layer is obtained from an empirical formula, as shown in equation (5):

$$k \geq \sqrt{j+m} + b \tag{5}$$

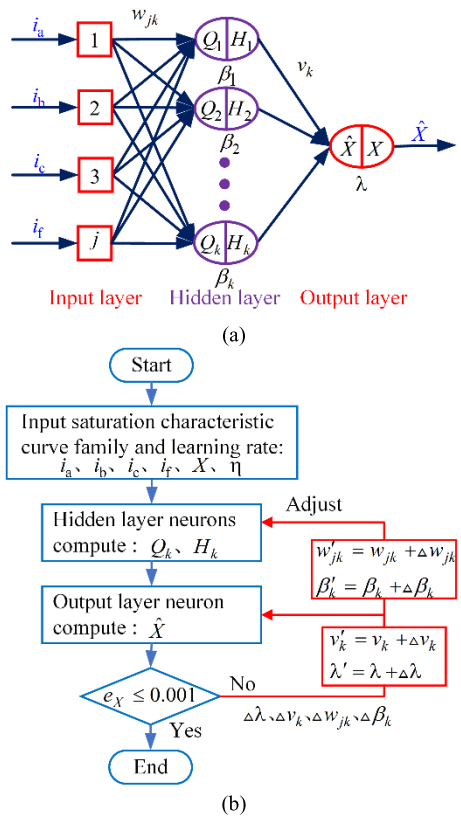

FIGURE 6. BP neural network model. (a) Structure of BP neural network. (b) Flow chart of BP neural network.

In equation (5), b is a constant and takes 10.

The computational flow of the BP neural network is shown in Fig. 6(b), where the input Q_k of the kth neuron in the hidden layer is:

$$Q_k = \begin{bmatrix} w_{1k} & w_{2k} & w_{3k} & w_{jk} \end{bmatrix} \begin{bmatrix} i_a \\ i_b \\ i_c \\ i_f \end{bmatrix} - \beta_k \tag{6}$$

In equation (6), the connection weights of the input and hidden layer neurons are w_{jk}, and the bias of the hidden layer neurons is β_k.

The hidden layer activation function is the Tansig function, and the output H_k of the kth neuron of the hidden layer is:

$$H_k = \frac{2}{1 + \exp(-2 \times Q_k)} - 1 \tag{7}$$

The output layer activation function is the Purelin function. Purelin functions are linear functions where the input equals the output. Then the time-varying reactance parameter $\hat{X}$ of the output layer is:

$$\hat{X} = g(i_a, i_b, i_c, i_f) = \begin{bmatrix} H_1 & H_2 & \cdots & H_k \end{bmatrix} \begin{bmatrix} v_1 \\ v_2 \\ \vdots \\ v_k \end{bmatrix} - \lambda \tag{8}$$

In equation (8), the connection weights of the hidden layer and output layer neurons are v_k, and the bias of the output layer neurons is λ.

The error e_X between the output value $\hat{X}$ and the desired value X of the reactance parameter is:

$$e_X = \frac{1}{2}(X - \hat{X})^2 \tag{9}$$

From Fig. 6(b), when error e_X does not satisfy the condition, the bias and weight of each layer are adjusted in reverse based on the error. The learning rate η is 0.01, and the adjustment value $\triangle\lambda$ for the output layer bias is:

$$\triangle\lambda = -\eta \frac{\partial e_X}{\partial \lambda} = -\eta(X - \hat{X}) \tag{10}$$

The adjusted value of the output layer weights $\triangle v_k$ is:

$$\triangle v_k = -\eta \frac{\partial e_X}{\partial v_k} = -\eta(-(X - \hat{X})H_k) \tag{11}$$

The adjusted value of the hidden layer bias $\triangle\beta_k$ is:

$$\triangle\beta_k = -\eta \frac{\partial e_X}{\partial \beta_k} = -\eta((X - \hat{X})v_k(1 + H_k)(1 - H_k)) \tag{12}$$

The adjusted value $\triangle w_{jk}$ of the hidden layer connection weight to the j input signal is:

$$\triangle w_{jk} = -\eta \frac{\partial e_X}{\partial w_{jk}} = -\eta((X - \hat{X})v_k(1 + H_k)(1 - H_k)i_f) \tag{13}$$

Equation (8) as a unified formula for the nonlinear function of reactance characterizes the time-varying reactance. The nonlinear functions of the different time-varying reactances correspond to different structural parameters of the net, which are obtained by iteratively training data sets. During the neural network training, 200 sets of data for each reactance parameter were selected as the training dataset, and 40 sets of data for each reactance parameter with drastic changes in saturation were chosen as the test dataset. As can be seen from Fig. 7, the errors for the different reactances are less than 0.4%. This error level indicates that the reactance neural network is well, and the resulting neural network model can be used as a nonlinear function of the reactance parameters.

III. TRANSIENT MATHEMATICAL MODEL OF SYNCHRONOUS CONDENSER BASED ON TIME-VARYING REACTANCE PARAMETERS

To accurately describe the SC transient operation process, the state equation is established based on the time-varying reactance obtained from BP neural network training, as shown in Equation (14):

$$\frac{d\hat{\boldsymbol{\psi}}}{dt} = \boldsymbol{u} - \boldsymbol{R}\boldsymbol{i} - \boldsymbol{w}\hat{\boldsymbol{\psi}} \tag{14}$$

In equation (14), $\boldsymbol{u}$, $\boldsymbol{i}$, and $\hat{\boldsymbol{\psi}}$ are the voltage, current, and magnetic flux vectors, respectively, and R is the resistance.

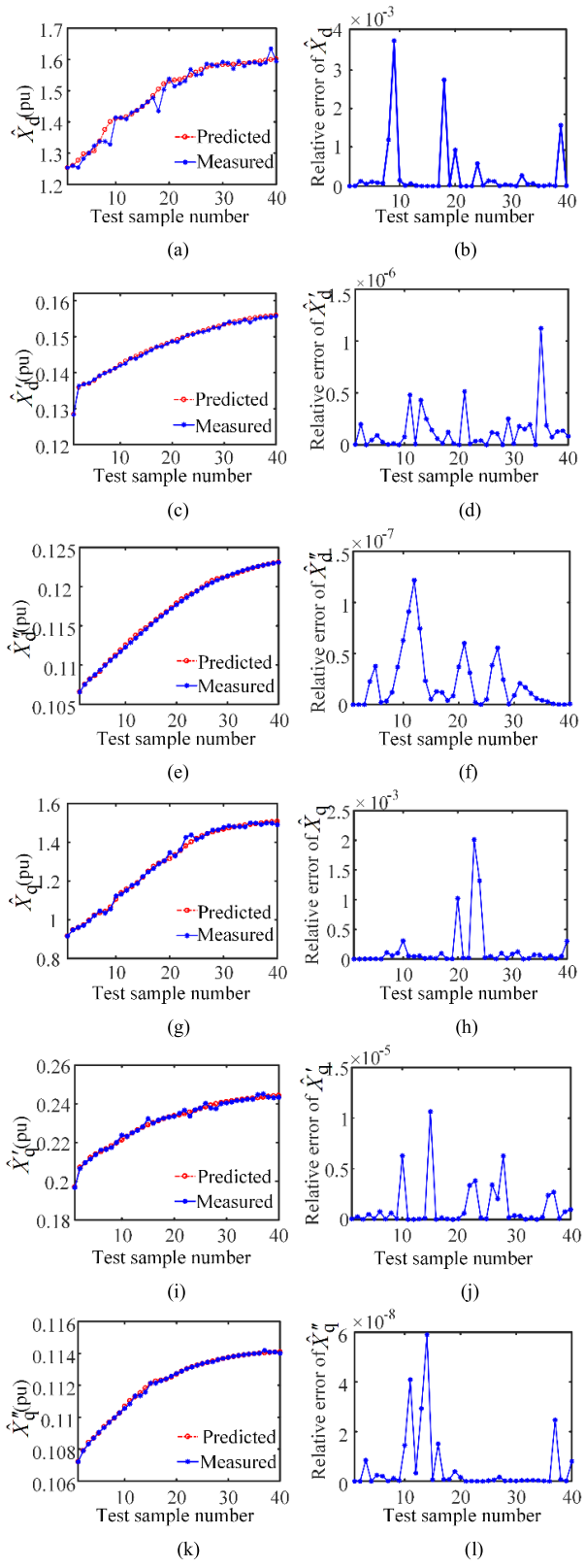

FIGURE 7. Results in BP neural network training. (a) Training result for $\hat{X}_{\mathrm{d}}$. (c) Training result for $\hat{X}_{\mathrm{q}}$. (e) Training result for $\hat{X}'_{\mathrm{d}}$. (g) Training result for $\hat{X}'_{\mathrm{q}}$. (i) Training result for $\hat{X}''_{\mathrm{d}}$. (k) Training result for $\hat{X}''_{\mathrm{q}}$. (b), (d), (f), (h), (j), and (l) are the relative error.

Where the time-varying reactance-based magnetic flux vector is shown in equation (15):

$$\begin{aligned}\hat{\boldsymbol{\psi}} &= \hat{\boldsymbol{X}}\boldsymbol{i} \\ &= \begin{bmatrix} \hat{X}_{\mathrm{d}} & 0 & \hat{X}_{\mathrm{ad}} & \hat{X}_{\mathrm{ad}} & 0 & 0 \\ 0 & \hat{X}_{\mathrm{q}} & 0 & 0 & \hat{X}_{\mathrm{aq}} & \hat{X}_{\mathrm{aq}} \\ \hat{X}_{\mathrm{ad}} & 0 & \hat{X}_{\mathrm{f}} & \hat{X}_{\mathrm{ad}} & 0 & 0 \\ \hat{X}_{\mathrm{ad}} & 0 & \hat{X}_{\mathrm{ad}} & \hat{X}_{\mathrm{D}} & 0 & 0 \\ 0 & \hat{X}_{\mathrm{aq}} & 0 & 0 & \hat{X}_{\mathrm{Q}} & \hat{X}_{\mathrm{aq}} \\ 0 & \hat{X}_{\mathrm{aq}} & 0 & 0 & \hat{X}_{\mathrm{aq}} & \hat{X}_{\mathrm{H}} \end{bmatrix} \begin{bmatrix} i_{\mathrm{d}} \\ i_{\mathrm{q}} \\ i_{\mathrm{f}} \\ i_{\mathrm{D}} \\ i_{\mathrm{Q}} \\ i_{\mathrm{H}} \end{bmatrix} \end{aligned} \tag{15}$$

In equation (15), $\hat{\boldsymbol{X}}$ is the d-axis and q-axis time-varying reactance, which consists of the reactance model obtained by training the BP neural network.

The time-varying field reactance $\hat{X}_{\mathrm{f}}$ is shown in equation (16):

$$\begin{cases} \hat{X}_{\mathrm{f}\sigma} = 1/(1/(\hat{X}'_{\mathrm{d}} - X_\sigma) - 1/\hat{X}_{\mathrm{ad}}) \\ \hat{X}_{\mathrm{f}} = \hat{X}_{\mathrm{f}\sigma} + X_{\mathrm{ad}} \end{cases} \tag{16}$$

where $\hat{X}_{\mathrm{f}\sigma}$ is the time-varying field leakage reactance, $\hat{X}_{\mathrm{ad}}$ is the time-varying d-axis armature reactance, and X_σ is the stator leakage reactance.

The time-varying d-axis damping reactance $\hat{X}_{\mathrm{D}}$ is shown in equation (17):

$$\begin{cases} \hat{X}_{\mathrm{D}\sigma} = 1/(1/(\hat{X}''_{\mathrm{d}} - X_\sigma) - 1/\hat{X}_{\mathrm{ad}} - 1/\hat{X}_{\mathrm{f}\sigma}) \\ \hat{X}_{\mathrm{D}} = \hat{X}_{\mathrm{D}\sigma} + X_{\mathrm{ad}} \end{cases} \tag{17}$$

where $\hat{X}_{\mathrm{D}\sigma}$ is the time-varying damping leakage reactance.

The time-varying q-axis damping circuit reactance $\hat{X}_{\mathrm{Q}}$ is:

$$\begin{cases} \hat{X}_{\mathrm{Q}\sigma} = 1/(1/(\hat{X}'_{\mathrm{q}} - X_\sigma) - 1/\hat{X}_{\mathrm{aq}}) \\ \hat{X}_{\mathrm{Q}} = \hat{X}_{\mathrm{aq}} + X_{\mathrm{Q}\sigma} \end{cases} \tag{18}$$

where $\hat{X}_{\mathrm{Q}\sigma}$ is the time-varying first equivalent damping leakage reactance.

The time-varying second equivalent q-axis damping circuit reactance $\hat{X}_{\mathrm{H}}$ is:

$$\begin{cases} \hat{X}_{\mathrm{H}\sigma} = 1/(1/(\hat{X}''_{\mathrm{q}} - X_\sigma) - 1/\hat{X}_{\mathrm{aq}} - 1/\hat{X}_{\mathrm{Q}\sigma}) \\ \hat{X}_{\mathrm{H}} = \hat{X}_{\mathrm{aq}} + X_{\mathrm{H}\sigma} \end{cases} \tag{19}$$

where $\hat{X}_{\mathrm{H}\sigma}$ is the time-varying second equivalent damping leakage reactance.

The block diagram of the SC equation of state is shown in Fig. 8. In Fig. 8, the time-varying transient reactance obtained from the BP neural network is transformed through equations (16)-(19) to get the time-varying reactance parameters in the state equation. When the condenser is in transient operation, the time-varying reactance parameters vary with the armature and field currents. Therefore, the proposed transient mathematical model is different from the traditional fixed-parameter mathematical model, which takes complete account of dynamic magnetic saturation, and can provide a more accurate calculation of the dynamic characteristics of the condenser.

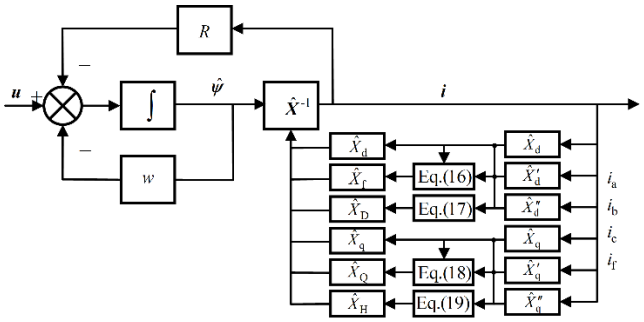

FIGURE 8. Block diagram of the equation of state for SC.

IV. VERIFICATION OF MATHEMATICAL MODEL

In this paper, a system simulation model with SC transient mathematical model is established using simulation software in the context of a UHVDC transmission system application, as shown in Fig. 9(a). The system model consists of the sending AC system, the sending rectifier station, the sending AC filter, the transmission line, the receiving AC system, the receiving inverter station, the receiving AC filter, the fault module, the SC conventional fixed parameter model (Model 1), the mathematical model proposed in this paper (Model 2), and saturated standard SG model (Model 3) used in power system. And the no-load characteristic saturation curve in Model 3 is the test value. Tables 1 and 2 give the basic parameters of the UHVDC transmission system and the prototype, respectively.

The block diagrams of Model 1, Model 2, and Model 3 operating in parallel on the transmission system is shown in Fig. 9(b). During the operation of the transmission system, the mathematical model of the SC uses the phase voltage of the system to update the phase currents injected into the system. There is a significant difference between Model 1, Model 2, and Model 3. The parameters in Model 1 are fixed. The parameters in Model 3 take into account the effect of saturation and are also fixed parameters, which are modified by the no-load characteristic saturation curve of the condenser. However, the parameters in Model 2 are time-varying. During operation, the system currents and excitation current are fed back to the parameter identification module to update Model 2, realizing that time-varying parameters change with operating conditions.

A. CALCULATION RESULTS

Model 1, Model 2 and Model 3 are used to simulate the same voltage sag fault on the AC system at the sending end of the transmission system. The fault start time is 0.0987s, the fault duration is 0.037s, and the fault end time is 0.1357s. The dynamic response comparison results of SC Model 1, Model 2 and Model 3 are shown are shown in Fig. 10.

In Fig. 10, the terminal voltage, field current, and the stator current represented by the A-phase winding current are different when the mathematical model considers the dynamic magnetic saturation effect than when it does not.

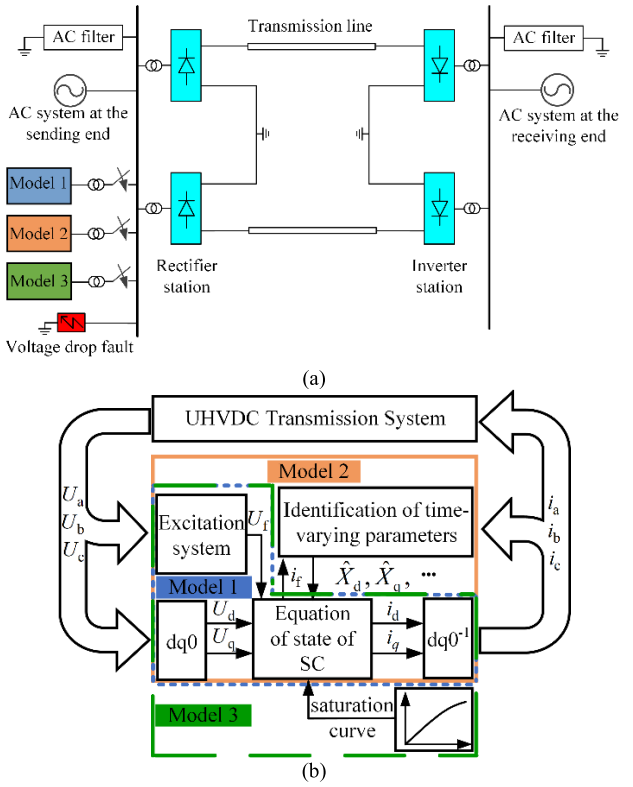

FIGURE 9. Simulation model. (a) Simulation model of UHVDC transmis-sion system. (b) Block diagram of Model 1, Model 2 and Model 3.

TABLE 1. Basic parameters of the UHVDC transmission system.

Parameter	Sending end	Receiving end
Rated voltage	530 kV	515 kV
Rated frequency	50 Hz	50 Hz
DC voltage	±800 kV	±800 kV
DC current	6.25 kA	6.25 kA
Maximum short-circuit capacity	57288 MVA	57288 MVA

In Fig. 10(d), the reactive power of Model 2 rises from 11.4 MVar to an instantaneous maximum reactive power of 456 MVar, the reactive power of Model 3 increased from 11.4 MVar to 494.4 MVar, and the reactive power of Model 1 rises from 11.4 MVar to an instantaneous maximum reactive power of 489 MVar. Model 1 is a fixed parameter model. The difference between the instantaneous maximum power of the proposed model and Model 1 is 33 MVar, and the difference between the instantaneous maximum power of Model 3 and Model 1 is 5.4 MVar. Therefore, the dynamic magnetic saturation effect significantly impacts the maximum reactive power output during SC transient operation.

To further analyze the dynamic magnetic saturation effect, the simulation results of the time-varying parameters of Model 2 during the voltage sag fault condition were extracted, as shown in Fig. 11.

As can be seen from the time-varying parameter variation law of Model 2 in Fig. 11, the time-varying parameters

TABLE 2. Basic parameters of prototype.

Parameter	Value
Rated capacity	300 MVar
Rated voltage	20000 V
Rated current	8660.3 A
No load field current	861 A
Rated frequency	50 Hz
Number of stator parallel branches	3
Number of phase belts	2

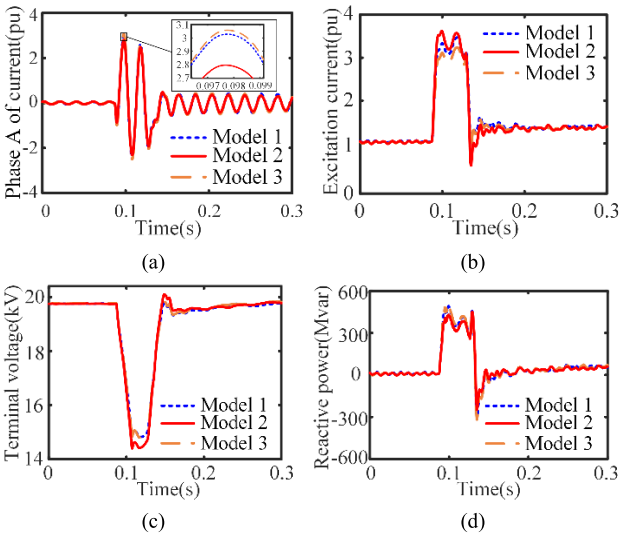

FIGURE 10. Transient response characteristics of the condenser. (a) Phase A current of SC. (b) Field current of SC. (c) Terminal votage of SC. (d) Reactive power of SC.

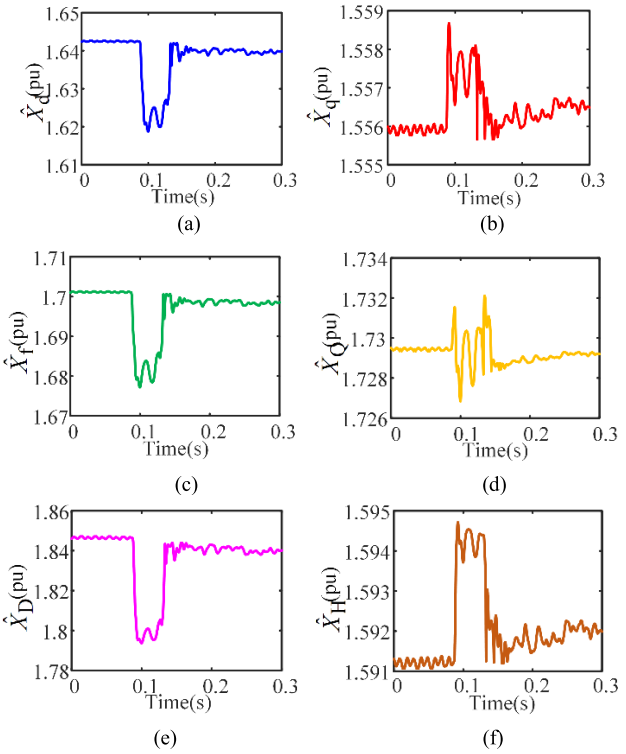

FIGURE 11. Time-varying parameters. (a) $\hat{X}_d$. (b)$\hat{X}_q$. (c) $\hat{X}_f$. (d) $\hat{X}_Q$.(e) $\hat{X}_D$. (f) $\hat{X}_H$.

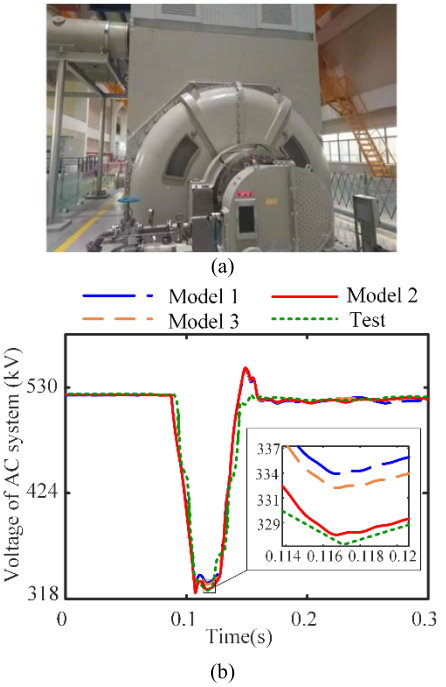

FIGURE 12. Comparison of simulation and test results under fault conditions. (a) Prototype of large-capacity synchronous condenser used in the test (b) Comparison results of AC system voltage.

are unchanged before a fault occurs and change with the operating conditions when a fault occurs.

Model 3 corrects the parameters during operation through the no-load characteristic saturation curve, and the parameters are not easily obtained directly. According to the comparison results in Fig. 10, the calculation results of Model 1 and Model 3 are relatively close. Therefore, the parameters of model 1 can be used as a representative to compare with the time-varying parameters of model 2 proposed in this paper. The results for the fixed parameters of Model 1 compared to the lowest point of the time-varying parameter changes of Model 2 are shown in Table 3. In Table 3, X_d, X_f, and X_D saturation change are more significant. X_q, X_Q, and X_H saturation change are minor. As a result, the d-axis parameters are more affected by the dynamic magnetic saturation effect, and the q-axis parameters are less affected by a system voltage sag fault.

B. TEST VERIFICATION

In order to verify the accuracy of the mathematical model, the calculated results of Model 1, Model 2 and Model 3 were compared with the field test results of the bus voltage at the sending end when a voltage sag fault occurred in the system, as shown in Fig. 12.

In Fig. 12(b), in the event of voltage sag fault at the sending end of the AC system, the calculation results of

TABLE 3. Comparison of parameters of different models.

Parameter	Model 1 (pu)	Model 2 (pu)	Saturation variation(%)
X_d	1.643	1.612	1.88
X_f	1.7	1.674	1.529
X_D	1.84	1.792	2.619
X_q	1.556	1.555	0.064
X_Q	1.723	1.722	0.058
X_H	1.592	1.591	0.063

the proposed mathematical model are compared with those of Model 1 and Model 3, and the results of the proposed mathematical model are closer to the actual measurement results. Compare the system voltage drop to the lowest point during the fault. The test-measured system voltage fell to 326.22 kV, the Model 1 system voltage dropped to 333.83 kV, the proposed model system voltage dropped to 327.31 kV, and the Model 3 system voltage fell to 332.29 kV. At this moment, the relative error between the calculated results of model 1 and the experimental measurements is 2.33%, the relative error between the computed results of the proposed mathematical model and the experimental measurements is 0.33%, and the relative error between the calculated results of model 3 and the experimental measurements is 1.86%. From the comparison results, it can be seen that the relative error of the proposed mathematical model is 2% less than that of the traditional fixed-parameter model and 1.53% less than that of the saturated standard SG model used in the power system. Therefore, the nonlinear transient mathematical model based on the time-varying reactance parameters proposed in this paper has higher computational accuracy.

V. CONCLUSION

A new mathematical model for the nonlinear transients of SC has been proposed in this paper. The model considers the effect of dynamic magnetic saturation on reactance parameters. And the calculation of the time-varying reactance parameters in the mathematical model has been presented in this paper. The accuracy of the proposed model was verified by comparing it with the results of the saturated standard SG model used in the power system, traditional fixed-parameter mathematical models, and field tests.

To further analyze the effect of dynamic magnetic saturation, the reactive power compensation results of the proposed mathematical model were compared with those of the traditional fixed-parameter model and saturated standard SG model used in the power system. The results show that the dynamic magnetic saturation effect significantly impacts the maximum reactive power output during SC transient operation. Moreover, the effect of dynamic magnetic saturation mainly affects the reactance parameter of the d-axis. As a result, the new transient mathematical model can accurately consider the dynamic magnetic saturation effect and is closer to the actual motor state. The model can be further applied for fault monitoring and diagnosis research where high model accuracy is required.

ACKNOWLEDGMENT

The authors would like to thank Harbin Electric Machinery Company Ltd., for their support of the research work in this article.

REFERENCES

[1] Y. T. Wang, Y. C. Zhang, Q. Y. Zhou, Z. Q. Li, Y. L. Jiang, Y. Tang, J. L. Wu, C. Gao, J. Z. Tu, and C. Shen, "Study on application of new generation large capacity synchronous condenser in power grid," *Power Syst. Technol.*, vol. 41, no. 1, pp. 22–28, Jan. 2017.

[2] Z. Y. Liu, Q. P. Zhang, Y. T. Wang, C. Dong, and Q. Y. Zhou, "Research on reactive compensation strategies for improving stability level of send-end of 750 kV grid in Northwest China," *Proc. CSEE*, vol. 35, no. 5, pp. 1015–1022, Mar. 2015.

[3] M. Cheng, W. J. Tian, W. Wang, and C. Wei, "Review on key technologies and latest development of new synchronous condenser," *Electr. Power Eng. Technol.*, vol. 39, no. 23, pp. 1–9, Mar. 2019.

[4] J. Jia, G. Yang, A. H. Nielsen, and P. Rønne-Hansen, "Impact of VSC control strategies and incorporation of synchronous condensers on distance protection under unbalanced faults," *IEEE Trans. Ind. Electron.*, vol. 66, no. 2, pp. 1108–1118, Feb. 2019.

[5] M. A. Jabbar, Z. Liu, and J. Dong, "Time-stepping finite-element analysis for the dynamic performance of a permanent magnet synchronous motor," *IEEE Trans. Magn.*, vol. 39, no. 5, pp. 2621–2623, Sep. 2003.

[6] J. Di, J. E. Fletcher, W. Li, H. Xu, and Y. Fan, "Transient analysis of line-start permanent magnet linear synchronous motors," *IEEE Trans. Energy Convers.*, vol. 36, no. 4, pp. 3365–3375, Dec. 2021.

[7] N. A. O. Demerdash and P. Baldassari, "A combined finite element-state space modeling environment for induction motors in the ABC frame of reference: The no-load condition," *IEEE Trans. Energy Convers.*, vol. 7, no. 4, pp. 698–709, Dec. 1992.

[8] T. J. Hammons and D. J. Winning, "Comparisons of synchronous-machine models in the study of the transient behaviour of electrical power systems," *Proc. Inst. Elect. Eng.*, vol. 118, no. 10, pp. 1442–1458, 1971.

[9] *Guide for Synchronous Generator Modeling Practices and Parameter Verification With Applications in Power System Stability Analyses*, IEEE Standard 1110-2019, 2019.

[10] P. W. Sauer, M. A. Pai, and J. H. Chow, *Power System Dynamics and Stability: With Synchrophasor Measurement and Power System Toolbox*, 2nd ed. Hoboken, NJ, USA: Wiley, 2018.

[11] D. C. Aliprantis, O. Wasynczuk, and C. D. R. Valdez, "A voltage-behind-reactance synchronous machine model with saturation and arbitrary rotor network representation," *IEEE Trans. Energy Convers.*, vol. 23, no. 2, pp. 499–508, Jun. 2008.

[12] Y. Zhang and A. M. Cramer, "Unified model formulations for synchronous machine model with saturation and arbitrary rotor network representation," *IEEE Trans. Energy Convers.*, vol. 31, no. 4, pp. 1356–1365, Dec. 2016.

[13] Z. Q. Li, Z. Y. Chong, and J. J. Huang, "Test verification of dynamic reactive power characteristics of fast dynamic response synchronous condenser," *Proc. CSEE*, vol. 39, no. 23, pp. 6877–6885 and 7101, Dec. 2019.

[14] Z. Q. Li, W. Y. Jiang, Y. B. Wang, W. F. Li, Z. K. Li, and Z. L. Xian, "Key technical parameters and optimal design of new types of large capacity synchronous condenser," *Large Electr. Mach. Hydraulic Turbine*, vol. 2017, no. 4, pp. 15–22, Apr. 2017.

[15] *Guide for Test Procedures for Synchronous Machines Part I—Acceptance and Performance Testing Part II—Test Procedures and Parameter Determination for Dynamic Analysis*, IEEE Standard 115-2009, 2009.

[16] F. S. Sellschopp and M. A. Arjona, "Semi-analytical method for determining *d*-axis synchronous generator parameters using the DC step voltage test," *IET Electr. Power Appl.*, vol. 1, no. 3, pp. 348–354, 2007.

[17] J. Bladh, M. Wallin, L. Saarinen, and U. Lundin, "Standstill frequency response test on a synchronous machine extended with damper bar measurements," *IEEE Trans. Energy Convers.*, vol. 31, no. 1, pp. 46–56, Mar. 2016.

[18] A. Belqorchi, U. Karaagac, J. Mahseredjian, and I. Kamwa, "Standstill frequency response test and validation of a large hydrogenerator," *IEEE Trans. Power Syst.*, vol. 34, no. 3, pp. 2261–2269, May 2019.

[19] F. Maurer, M. T. Xuan, and J.-J. Simond, "Two full parameter identification methods for synchronous machine applying DC-decay tests for a rotor in arbitrary position," *IEEE Trans. Ind. Appl.*, vol. 53, no. 4, pp. 3505–3518, Jul. 2017.
[20] Y. Ma, L. Zhou, and J. Wang, "Standstill time-domain response parameter estimation of the large synchronous condenser in arbitrary rotor position," *IEEE Access*, vol. 8, pp. 166047–166059, 2020.
[21] Y. Ma, J. Wang, Y. Xiao, L. Zhou, and Z. Q. Zhu, "Two-level surrogate-assisted transient parameters design optimization of a wound-field synchronous machine," *IEEE Trans. Energy Convers.*, vol. 37, no. 1, pp. 737–747, Mar. 2022.

XIAO HAN was born in Hebei, China, in 1993. She is currently pursuing the Ph.D. degree in electrical machine with the Harbin University of Science and Technology, Harbin, China.

Her research interests include electromagnetic, operation analysis, and the design of large electrical machines.

YANPING LIANG was born in Harbin, China, in 1963. She received the M.S. degree in electrical machine from the Harbin University of Science and Technology, Harbin, in 1988, and the Ph.D. degree in electrical machine from the Harbin Institute of Technology, Harbin, in 2005.

She is currently a Professor with the Harbin University of Science and Technology. Her research interests include electrical machine electromagnetic theory and design, large generator electromechanical energy conversion, and electromagnetic field calculation.

ERHANG ZHU was born in Hebei, China, in 1991. He is currently pursuing the Ph.D. degree in electrical machine with the Harbin University of Science and Technology, Harbin, China.

His research interests include electromagnetic, operation analysis, and the design of large electrical machines.

XU BIAN was born in Harbin, China, in 1988. She received the B.S., M.S., and Ph.D. degrees in electrical machine from the Harbin University of Science and Technology, Harbin, in 2010, 2013, and 2016, respectively.

She is currently a Professor with the Harbin University of Science and Technology. Her research interests include electromagnetic, fluid and thermal analysis, and the design of electrical machines.